Nationaal Lucht- en Ruimtevaartlaboratorium

National Aerospace Laboratory NLR

NLR-TP-2004-167

Determination of Absolute Contributions of Aircraft Noise Components using Fly-Over Array Measurements

P. Sijtsma and R.W. Stoker*

* The Boeing Company

This report has been based on AIAA Paper 2004-2958 presented at the 10th AIAA/CEAS Aerocoustics Conference, at Manchester, UK on 10-12 May, 2004.

Customer:	National Aerospace Laboratory NLR
Working Plan number:	AV.1.C.1
Owner:	National Aerospace Laboratory NLR
Division:	Aerospace Vehicles
Distribution:	Unlimited
Classification title:	Unclassified
	April 2004

Approved by author:	Approved by project manager:	Approved by project managing department:
14/5/04	4/6/04	15/6

Summary

For wind tunnel array measurements, the source power integration technique has proved to be a valuable technique to determine absolute source levels. This paper describes the extension of the source power integration technique to moving sources, and the application to fly-over array measurements on landing aircraft at Amsterdam Airport Schiphol. The technique is applied in combination with a modified version of the Delay-and-Sum beamforming technique, which includes microphone- and frequency-dependent weight factors. These weight factors are used to correct for microphone spatial density and to account for the effects of coherence loss. This beamforming technique works well in combination with the array design, which consists of a number of concentric rings of microphones, with increasing density towards the center. In this paper, it is demonstrated that the extended source power integration technique is able to determine absolute levels from fly-over array measurements, when it is used in combination with the special beamforming technique and the Schiphol array design. Thus, absolute quantification of difference source regions on an aircraft is feasible. Microphone auto-correlations must be included in the beamforming process in order to obtain correct integrated levels, although acoustic images look better when beamforming is done without auto-correlations. The source power integration technique is applied to a Boeing 737-400, and to an Airbus A340.

Contents

1 Table
14 Figures

(26 pages in total)

Nomenclature

A_j	=	source power
f_j	=	frequency
j	=	frequency index
m,n	=	microphone indices
N	=	number of microphones
R_j	=	effective array radius
r_n	=	distance to the array midpoint
t	=	time
t_n	=	reception time at *n*-th microphone
T_n	=	transfer function
$w_{n,j}$	=	microphone weight
W	=	effective array radius at 4000 Hz
Z	=	dynamic range of source power integration
$\chi_n(t)$	=	fluctuating pressure measured by n-th microphone
$\sigma(t)$	=	source signal
$\tilde{\sigma}(t)$	=	estimated source signal
τ	=	emission time
$\vec{\xi}(t)$	=	position of moving source
Ω	=	spatial window function
$\vec{\Im}$	=	Fourier transform

1 Introduction

In the last decade, microphone arrays have become more and more in use as a standard tool for acoustic source location. The increasing capacity of computers and data acquisition systems have enabled the use of large numbers of microphones, long acquisition times and high sample frequencies[1]. Microphone arrays can be applied to stationary sources, but also to moving sources. Sound source location on moving objects has been applied to rotating sources in wind tunnels[2] to trains passing by[3,4], and to aircraft flying over[5-7].

Aircraft fly-over array measurements can be used to investigate the noise of several airframe noise components and to assess the model scale effects of wind tunnel measurements[7].

Moreover, fly-over array measurements can be valuable for making a breakdown of all possible noise sources, including engine noise, so that their relative contributions to the total noise perceived on the ground is known.

Making a noise source breakdown means determination of absolute acoustic source levels for each individual source. Using conventional beamforming, the absolute source levels can be related to the peak levels of the source spots. However, this relation is only valid if the noise sources are compact, and if all microphones receive similarly shaped signals from that source. In reality, the noise source regions are often extended. Furthermore, during propagation from source to microphones, the source signals are distorted by atmospheric turbulence. This distortion is different from microphone to microphone, thus inducing loss of coherence[8], which results in reduction of peak levels.

The above-described complications are comparable to wind tunnel array measurement in open test sections. Here, the shear layer between the wind tunnel model and the (out-of-flow) array is the cause of the coherence loss. Brooks and Humphreys[9] showed that correct source levels can nevertheless be obtained by applying the “source power integration technique”. This technique sums the source power estimates, obtained by beamforming, in (part of) an acoustic image, and corrects the results with a scaling factor that was obtained by performing a simulation with a monopole point source.

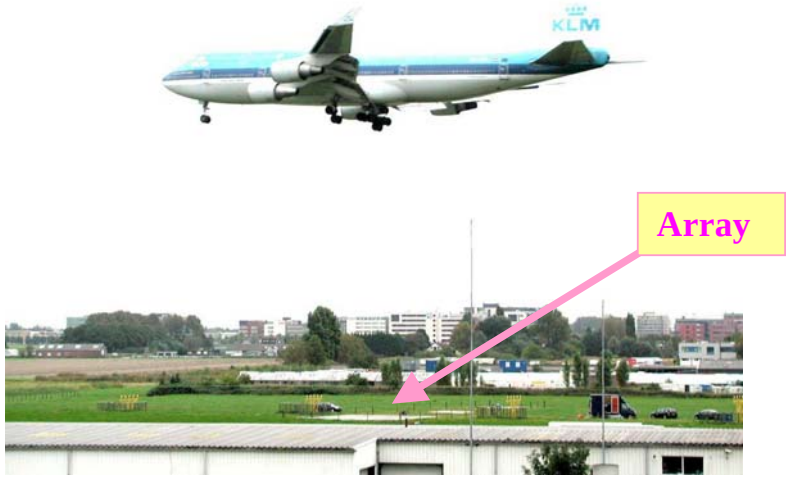

Figure 1: Array measurements at Schiphol Airport

The subject of this paper is the extension of this source power integration technique to array measurements on moving sources. The technique is applied to fly-over measurements on landing aircraft, performed in September 2002 at Amsterdam Airport Schiphol. During three days of measurements, 381 fly-over events were recorded with an array of 243 microphones, located within a circle of 6 m radius. The array was situated at a distance of about 750 m from the threshold of one of the runways. The measurements included many aircraft types. The average fly-over altitude was 43 m, the average speed was 68 m/s. The speed and the altitude of the airplanes were determined by a set of light sensors. This light sensor technique enabled an efficient, automatic determination of speed and height, without the cumbersome manual processing that is needed with for instance video cameras[10].
In this paper, a description is given of the beamforming technique, and, closely connected, the array design. Then, the beamforming technique is applied for source location on a landing Boeing 737-400. Next, the source power integration technique for moving sources is described. This new technique is applied to the same Boeing 737, and to an Airbus A340.

2 Beamforming

2.1 Source description

The beamforming algorithm that we used is based on the following sound transfer description from a moving sound source above the array to the microphones on the ground. Suppose that a point source moves with time-dependent position $\vec{\xi}(t)$, while emitting a sound signal $\sigma(t)$. The N microphones on the ground, located in $\vec{x}_n$, $n=1...N$, record the induced acoustic pressures $\chi_n(t)$. The relation between emitted and measured sound is:

$$\chi_n(t_n) = T_n(t_n,\tau)\sigma(\tau)\,, \tag{1}$$

where τ is the (fixed) emission time and t_n is the (microphone-dependent) receiving time. The transfer function T_n, which is based on a sound field description of a monopole source moving in a homogeneous atmosphere at rest[11], is given by

$$T_n(t_n,\tau) = 1\Big/ 4\pi\left\{\left\|\vec{x}_n - \vec{\xi}(\tau)\right\| - \frac{1}{c}\vec{\xi}'(\tau)\cdot\left(\vec{x}_n - \vec{\xi}(\tau)\right)\right\}, \tag{2}$$

where c is the speed of sound. The relation between emission and receiving time is:

$$t_n - \tau = \left\|\vec{x}_n - \vec{\xi}(\tau)\right\|\Big/ c\,. \tag{3}$$

2.2 Delay-and-Sum beamforming

A source signal $\tilde{\sigma}(\tau)$ can be reconstructed from (1) with the Delay-and-Sum procedure:

$$\tilde{\sigma}(\tau) = \frac{1}{N}\sum_{n=1}^{N}\tilde{\sigma}_n(\tau)\,, \tag{4}$$

where

$$\tilde{\sigma}_n(\tau) = \chi_n(t_n)/T_n(t_n,\tau)\,. \tag{5}$$

Clearly, when the moving focus $\vec{\xi}(t)$, i.e., the assumed source path that is used to calculate T_n, coincides with an actual moving monopole source, we find $\tilde{\sigma}(\tau) = \sigma(\tau)$. If there is a mismatch between moving focus and moving source, we usually have $\left|\tilde{\sigma}(\tau)\right| < \left|\sigma(\tau)\right|$.

2.3 Standard source power estimation (beamforming+AC)

A straightforward way to calculate the frequency spectrum of a source signal is evaluating Eq. (4) for $\tau = k\times\Delta t,\ k = 1...K,$ and then performing a discrete Fourier transform (DFT):

$$\vec{\Im}(\tilde{\sigma}) = \frac{1}{N}\sum_{n=1}^{N}\vec{\Im}(\tilde{\sigma}_n)\,. \tag{6}$$

The DFT result $\vec{\Im}$ is written here in vector notation. The individual components $\Im_j$ are the spectral results at the frequencies:

$$f_j = j/\Delta t,\ j = 1\cdots K/2-1 \tag{7}$$

The source power spectrum $A_j,\ j = 1,\ldots,K/2-1,$ is calculated as follows:

$$A_j = \frac{1}{2}\left|\Im_j(\tilde{\sigma})\right|^2 = \frac{1}{2N^2}\left|\sum_{n=1}^{N}\Im_j(\tilde{\sigma}_n)\right|^2 = \frac{1}{2N^2}\sum_{n=1}^{N}\sum_{m=1}^{N}\Im_j(\tilde{\sigma}_n)\Im_j(\tilde{\sigma}_m)^*, \tag{8}$$

in which the asterisk denotes complex conjugation.
Since the expression (8) includes the use of auto-correlations ($m = n$), we refer to this method as "beamforming+AC", in contrast with "beamforming–AC", which is described in the following section.

2.4 Source power estimation without using microphone auto-correlations (beamforming–AC)

If the microphone signals suffer from relatively high incoherent noise levels (e.g. wind noise), then the following approximation of (8) may be considered

$$A_j = \frac{1}{2N(N-1)}\sum_{n=1}^{N}\sum_{\substack{m=1\\m\neq n}}^{N}\Im_j(\tilde{\sigma}_n)\Im_j(\tilde{\sigma}_m)^* = \frac{1}{2N(N-1)}\left(\left|\sum_{n=1}^{N}\Im_j(\tilde{\sigma}_n)\right|^2 - \sum_{n=1}^{N}\left|\Im_j(\tilde{\sigma}_n)\right|^2\right). \tag{9}$$

This alternative method is analogous to the elimination of the main diagonal from the cross-correlation matrix in conventional beamforming techniques. Using this method, better looking acoustic images can be produced when microphone auto-correlations are relatively high compared to the cross-correlations. This may happen when the measurements are polluted by wind noise, or by loss of coherence. A caution to this method is that the source powers as calculated by (9) may have negative values. Since negative source powers are not physical, such results must be rejected.

2.5 Weight factors

It is possible to apply n-dependent weight factors $w_{j,n}$ (i.e., a spatial window), in the foregoing estimations of source power spectra. These weights may be frequency (j) dependent. Equations (8) and (9) then, respectively, change into:

$$A_j = \frac{1}{2}\sum_{n=1}^{N}\sum_{m=1}^{N} w_{j,n}w_{j,m}\Im_j(\tilde{\sigma}_n)\Im_j(\tilde{\sigma}_m)^* \Bigg/ \sum_{n=1}^{N}\sum_{m=1}^{N} w_{j,n}w_{j,m}\,, \tag{10}$$

$$A_j = \frac{1}{2}\sum_{n=1}^{N}\sum_{\substack{m=1\\m\neq n}}^{N} w_{j,n}w_{j,m}\Im_j(\tilde{\sigma}_n)\Im_j(\tilde{\sigma}_m)^* \Bigg/ \sum_{n=1}^{N}\sum_{\substack{m=1\\m\neq n}}^{N} w_{j,n}w_{j,m}\,. \tag{11}$$

3 Array design

The array was designed to have good performance in the frequency range 500 - 6000 Hz. In this range the array is required to have high array gain (low side lobe levels) and high resolution (narrow beam widths). The maximum radius for the microphone array was 6 m. The number of data channels available for microphones was 243.

3.1 Loss of coherence

In a previous measurement campaign at Schiphol Airport (September 2000) it was found that the array resolution is limited by loss of coherence due to atmospheric turbulence[8,12]. During propagation from noise sources on the aircraft to microphones on the ground, the sound signals are distorted by this turbulence. The distortion is different from microphone to microphone, so that coherence between different microphone signals is (partly) lost. Loss of coherence becomes increasingly significant for increasing distance between microphones, and for increasing frequency. For high frequencies, the outer microphones of the array have become completely incoherent with the other microphones, and thus the effective aperture of the array has become smaller than its physical size.

Quantifying the coherence loss is difficult. In the literature, there is no description of coherence loss of sound that propagates in vertical direction through the atmosphere. Also, it can not be deduced immediately from the fly-over measurements. Assessment of coherence loss would have been possible through single source measurements at an altitude of 40 m above the array, but such a test would incur practical problems (e.g. at the test site it would be impossible for safety reasons).

Indirectly, loss of coherence can be perceived from the fly-over measurements. This is done by processing array data of a single fly-over event with different array sizes[9], and comparing the resultant acoustic images. First, an array processing can be done with the entire array, and then the outer part of the array can be excluded from the processing. If the outer microphones are affected by loss of coherence, they do not contribute effectively to the beamforming process, but they only add noise. Reduction of array size will then not result into lower resolution, but the peak levels will increase and the noise levels in the acoustic images will decrease.

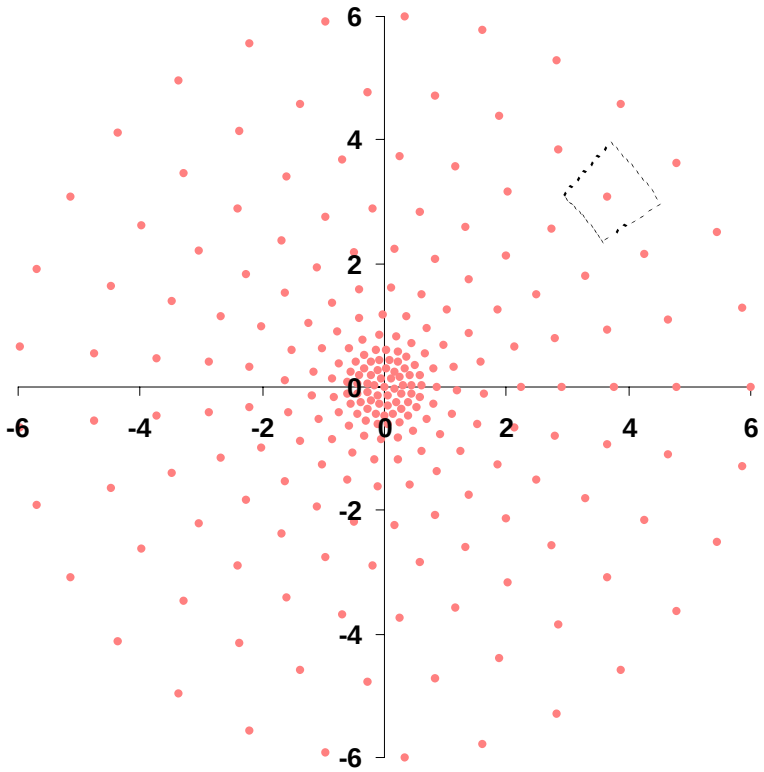

Figure 2: Microphone layout & area association

By performing such a study with different array sizes, using data from the previous Schiphol measurement campaign, it was found that the radius of the effective array aperture is, approximately:

$$R_j = 4000/f_j \ . \tag{12}$$

In other words, the effective array aperture at 4000 Hz is approximately a disk of 1 m radius. At other frequencies the empirically found effective array radius is inverse proportional to the frequency.

In order to have high array gain at the entire frequency range of interest, it is required to have available a sufficiently large number of microphones for each frequency. This holds in particular for the highest frequencies, where the effective array aperture (12) is small. Therefore, an array design was made with a high microphone density in the central part of the array, and more sparsely spaced microphones in the periphery (see Figure 2). The effects of frequency-dependent effective array apertures were incorporated in the beamforming process, by applying the following weight factors (see Section.2.2.5):

$$w_{n,j} = \Omega\left(\frac{r_n}{R_j}\right) = \frac{1}{2}\left\{1 - \mathrm{Erf}\left[8\left(\frac{r_n}{R_j} - 1\right)\right]\right\}, \tag{13}$$

where 'Erf" is the Error function and r_n is the distance to the midpoint of the array. The "spatial window" function Ω is illustrated in Figure 3.

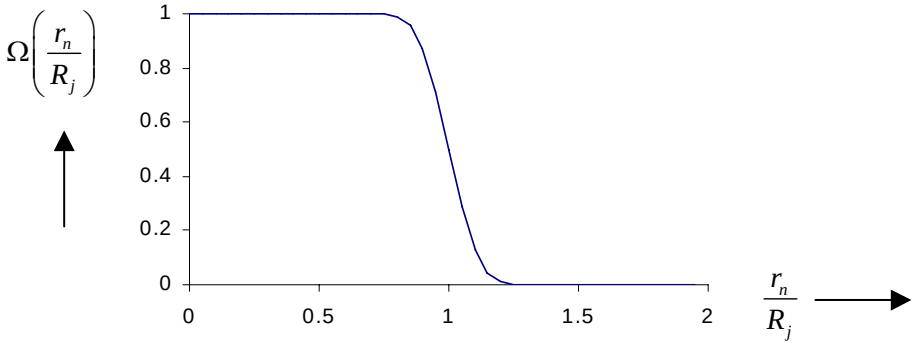

Figure 3: Illustration of Eq. (13)

3.2 Resolution

A drawback of an array design with densely spaced microphones in the central part, and more sparsely spaced microphones in the outer part, is that the array resolution is not optimal. If all microphones are processed with the same weight, then too much emphasis is put on the central part. Consequently, the array resolution is less than the resolution of a comparable continuous disk (or elliptic mirror) of the same size.

The above-mentioned drawback can be countered by associating each microphone (*n*) with a surrounding area, say λ_n^2 (m^2). These areas can be incorporated in the weight factors (13) as follows:

$$w_{n,j} = \lambda_n \Omega\left(\frac{r_n}{R_j}\right) = \frac{1}{2}\lambda_n\left\{1 - \mathrm{Erf}\left[8\left(\frac{r_n}{R_j} - 1\right)\right]\right\} \tag{14}$$

The weights λ_n are such that the processed acoustic power per unit area is approximately constant.

The array design (Figure 2) is such that this microphone-dependent area association is indeed possible. The array is built up by a number of concentric rings with increasing spacing towards the outer part. The spacing between rings is kept, as much as possible, the same as the spacing between two adjacent microphones in a ring. Thus, an area association is straightforward, as illustrated in Figure 2.

3.3 Properties

Using the beamforming–AC algorithm (11) with the weight factors (14), the array design has the following properties:

- Below 6300 Hz, the dynamic range (difference between peak level and highest side lobe level) is about 12 dB, in a scanning area of 80×80 m2, 40 m above the array.
- Due to the frequency-dependent spatial windowing (13), the lobe widths are constant for a large range of frequencies. At 40 m altitude, the spatial resolution of the array is 2 m, for 667 Hz and higher. Below 667 Hz, the resolution is inverse proportional to the frequency.

4 Example: Boeing 737-400

4.1 Acoustic images

One of the many aircraft types that were measured was the Boeing 737-400. This older B737 type is interesting for parametric studies on the array technique, because its noise is almost fully dominated by the engine exhausts. In this paper, we consider a B737-400 that flew over the array at an altitude of 40 m, and a speed of 76 m/s. Acoustic images were made using the beamforming technique described in the previous chapters (including the microphone weights (14) with (12). Source powers were estimated with beamforming+AC (Section 2.2.3) and beamforming–AC (Section 2.2.4). The data were averaged over a short period of 0.1 s of emission time, in which the engines were (on average) just above the array. Thus, the estimated source powers could be well compared with the sound levels of the microphones, without having to correct for Doppler frequency shift.

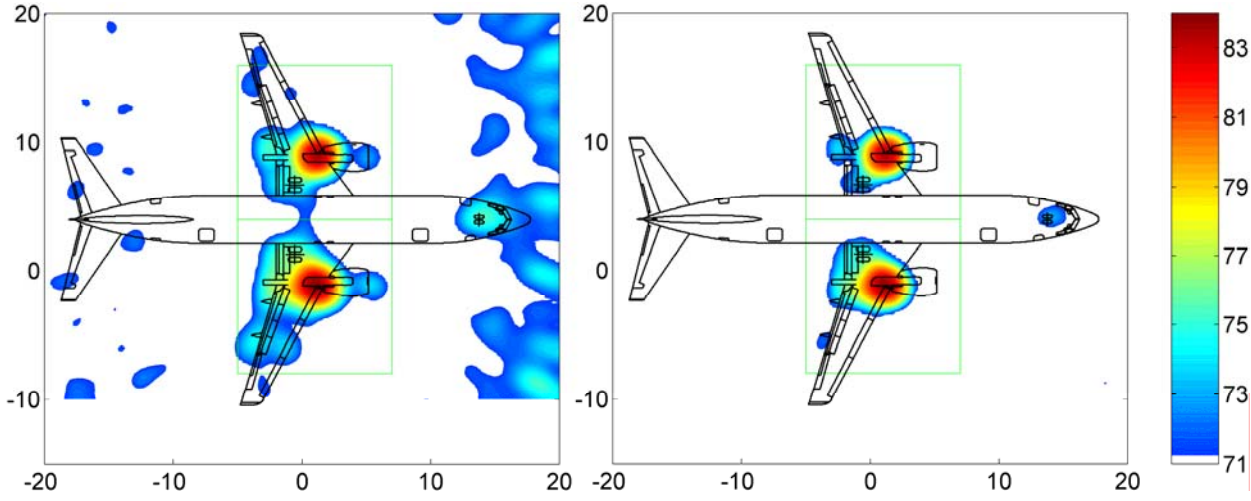

Figure 4: Acoustic images of B737-400 at 2000 Hz (1/3 octave band); left image: beamforming+AC, right image: beamforming–AC

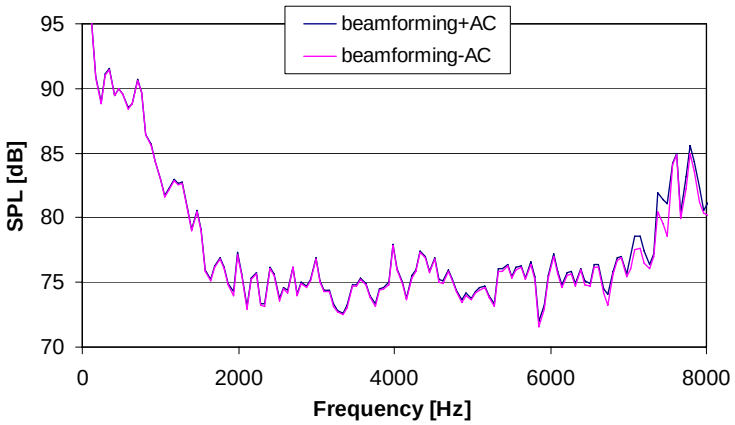

Figure 5: Narrow-band peak levels of acoustic images

In Figure 4, acoustic images, obtained with and without using auto-correlations, are shown at 2000 Hz (summed over a number of narrow-band source power results to obtain a 1/3 octave band result). The shown levels are corrected for distance between aircraft and array, such that they can be compared directly to the microphone levels. Comparing the different techniques, the following observations can be made:

- Without using auto-correlations, spurious sources (side lobes) have been disappeared in the image.
- Some true sources (engine inlets, slats) seem to have been disappeared as well.
- The levels of some other sources (flaps, nose gear) are decreased.
- The levels of the main sources (engine exhausts) seem to be unaffected.

The latter observation can be confirmed by comparing, for both methods, narrow-band plots of the peak levels of the images. This comparison is made in Figure 5, which shows, at a large range of frequencies, a negligible difference between both methods. It is remarked that, above 7000 Hz, the narrow-band peak locations not always coincide with the engine exhausts. Occasionally, spurious sources have higher levels than the actual sources.

4.2 Peak levels in acoustic images versus microphone levels

Peak levels in acoustic images correspond with true source levels if the following conditions are fulfilled:

a) the sources are point sources,
b) the resolution of the beamforming method is high enough to separate different sources,
c) there is no loss of coherence.

If we restrict ourselves to the engine exhausts, then condition b) seems to be fulfilled. Using the microphone weights (14) with (12), the effects of coherence loss may be suppressed sufficiently to fulfil condition c). Condition a), however, may be violated because the resolution (2 m) is not

large compared to the size of the sources (engine diameter). In other words, the point source assumption may not be valid here.

If the peak levels in the images *would* correspond to the actual source levels, then it would be likely that these peak levels, summed over both engines, agree with the average microphone levels. Such a comparison is made in Figure 6, in which the peak levels were determined as the maximum levels in the areas designated by the green boxes in Figure 4. For a fair comparison the microphone levels were averaged using the same weights (14). This figure demonstrates that the total source level is underpredicted by approximately 4 dB. The most likely reason is the violation of the point source assumption.

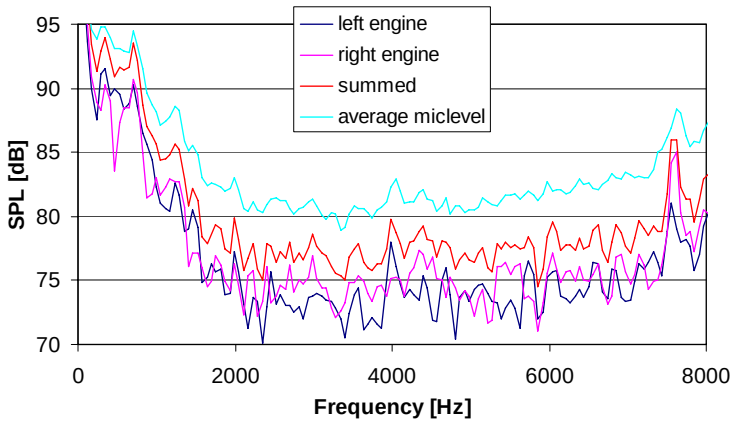

Figure 6: Narrow-band peak levels vs microphone levels

4.3 Variation of effective array radius

A possibility to get closer to the true source levels, is to decrease the effective array radius R_j, i.e., to make it smaller than (12). Then, the array resolution will be larger than 2 m, and consequently the engine exhaust noise sources better resemble point sources. Variation of effective array radius will be realized by introducing a parameter W in the relation between R_j and f_j:

$$R_j = W \times 4000 / f_j \,. \tag{15}$$

Thus, W is the effective array radius at 4000 Hz.

Using conventional beamforming, acoustic images were calculated for several values of W, ranging from 0.4 to 3.0 m, with 0.2 m increment. Values of W lower than 0.4 m incurred practical problems, because then the number of microphones is too small at high frequencies. Moreover, the source spots of both engines are no longer well separated.

Peak levels of the left engines for all these values of W are plotted in Figure 7. A strong dependency on array size is shown, thereby confirming the wind tunnel findings of Brooks and Humphreys[9]. As expected, the peak levels increase with decreasing effective array size. But

even at the lowest value of W, the peak levels are not high enough to predict the total noise level. This is demonstrated in Figure 8, where for W = 0.4 the peak levels of both engines, as well as and their sums, are plotted against average microphone levels. Probably, the point source assumption is still violated at W = 0.4.

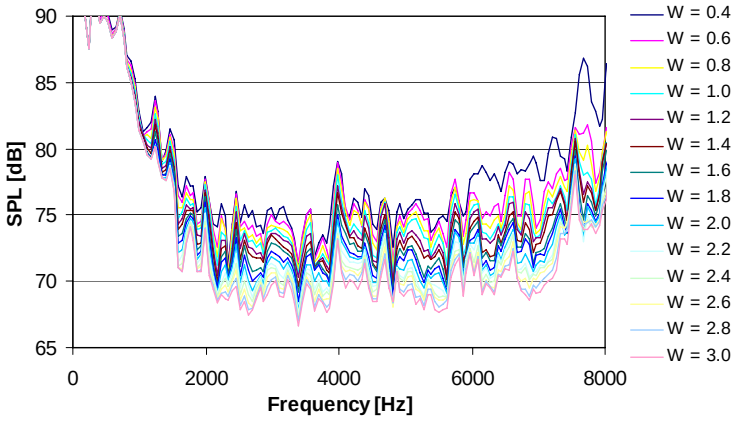

Figure 7: Narrow-band peak levels of left engine for several values of W

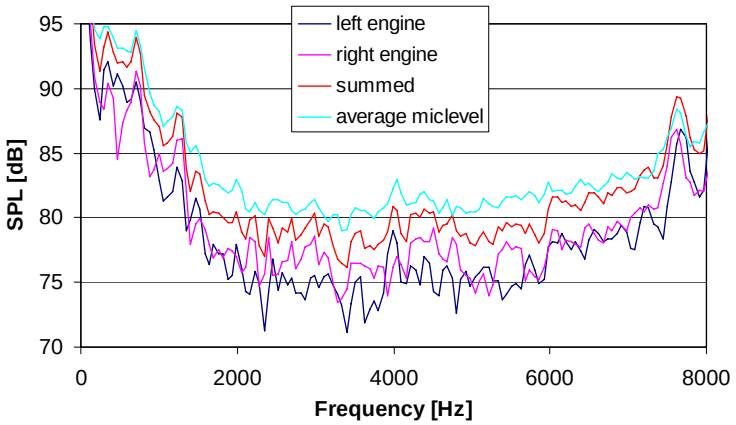

Figure 8: Narrow-band peak levels vs microphone levels for W = *0.4*

5 Source power integration

5.1 Description of technique

Problems with non-compact sources and coherence loss also occur in wind tunnel array measurements. To obtain absolute levels nonetheless, a source power integration technique was developed[9]. Basically, the integration technique sums the source power estimates for all points of a scan grid. Afterwards, the result is scaled such that the exact result is obtained for a simulated monopole source in the center of the grid. In more detail, the technique is as follows.

Suppose H is the number of points in a scan grid, and A_h, $h=1,...,H$, are the beamforming results (source power estimates) from measurements. Suppose further that $A_{s,h}$, $h=1,...,H$, are the beamforming results of a simulated monopole source with acoustic power P_s, in the center of the grid. Then, the integrated source power estimate is:

$$P = P_s \times \sum_{h=1}^{H} A_h \Big/ \sum_{h=1}^{H} A_{s,h} \,. \tag{16}$$

A more refined method considers only the source power estimates that are less than Z dB (dependent on array gain) below the respective peak levels $A_{\max}$ and $A_{s,\max}$. In other words, power estimates that are more than Z dB below the peak values are neglected. Thus, we have for the integrated source power:

$$P = P_s \times \sum_{h=1}^{H} B_h \Big/ \sum_{h=1}^{H} B_{s,h} \,, \tag{17}$$

where

$$B_h = \begin{cases} 0, \text{ if } 10^{10}\log\left(A_h / A_{\max}\right) \le -Z, \\ A_h, \text{ otherwise,} \end{cases} \tag{18}$$

and

$$B_{s,h} = \begin{cases} 0, \text{ if } 10^{10}\log\left(A_{s,h} / A_{s,\max}\right) \le -Z, \\ A_{s,h}, \text{ otherwise.} \end{cases} \tag{19}$$

This method can be applied to beamforming+AC and beamforming–AC results, as long as A_h and $A_{s,h}$ have been calculated with the same method. When beamforming–AC is used, then B_h must be set to zero when A_h is less than zero. The same holds for $B_{s,h}$ when $A_{s,h}$ is less than zero.

5.2 Extension to moving sources

The extension of the source integration technique to moving sources is straightforward. The same equations as above can be used. However, since the scan grid is moving, the monopole should be moving also. But when the integration time is short, the position of the monopole source can be centered in space *and* in time. Then, the simulations can be done with a stationary monopole.

5.3 Application to B737-400

The source power integration method is applied to the same B737-400 measurements as in the previous chapter. The integration is carried out over the region enclosed by the green lines in Figure 4. The results are split in a “left engine” and a “right engine” part, as indicated in Figure 4. Beamforming+AC was applied, as well as beamforming–AC. The same range of values of W was used in the beamforming algorithms as in Section 4.0. For the dynamic range Z of the source power integration technique we chose Z = 12 dB, but the results are not very sensitive to Z.

In Figure 9, the integrated source powers, obtained with beamforming+AC, are plotted for the left engine. From the source power integration technique, we would expect results that are independent on array size[9]. However, Figure 9 shows that the method seems to fail for large values of W. Apparently, the large effective array sizes result into too much coherence loss. An increase in coherence loss leads to an increase in noise floor levels in the acoustic images, and thus to integrated levels that are too high. Better results are obtained if the effective array radius (15) remains close to the empirical values defined by $W \approx 1$. This is demonstrated in Figure 10, where the same results are shown as in Figure 9, but now only for $W \leq 1.4$. This time, the integrated results are more independent of W.

In Figure 11, again integrated results are plotted, only these are obtained from beamforming–AC results. In this figure, the spectra are fairly independent of W. This is because acoustic images obtained by beamforming–AC suffer relatively little from noise floors. Comparing Figure 10 with Figure 11, it seems that the results obtained with beamforming–AC are a few dB lower than with the beamforming+AC technique. To examine which method provides the best answers, the integrated results over the total integration area (left engine and right engine) are compared with the average microphone levels. This is done for the “standard” effective array radius (12), corresponding to W = 1.0. The results are shown in Figure 12. Clearly, beamforming+AC gives the best results. Apparently, beamforming–AC suppresses the secondary sources too much, which could already be observed in Figure 4.

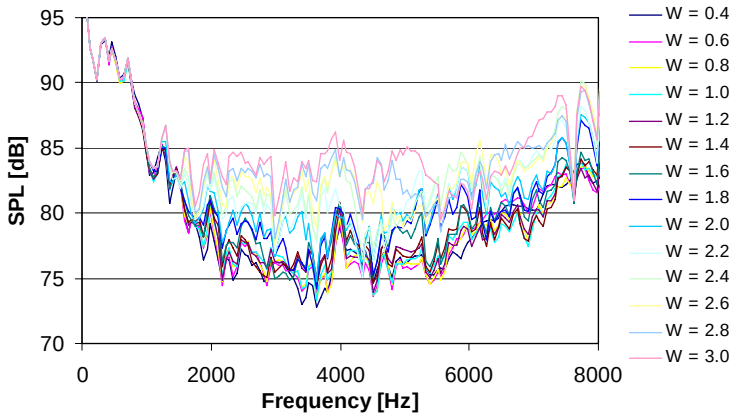

Figure 9: Integrated source powers of left engine for several values of W*; beamforming+AC*

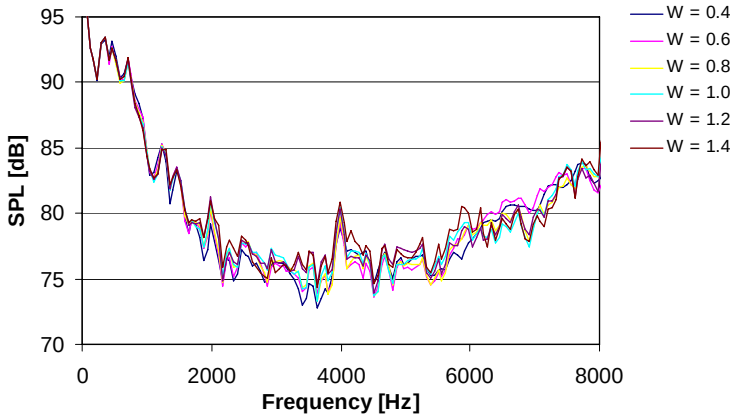

Figure 10: Integrated source powers of left engine for W *≤1.4; beamforming+AC*

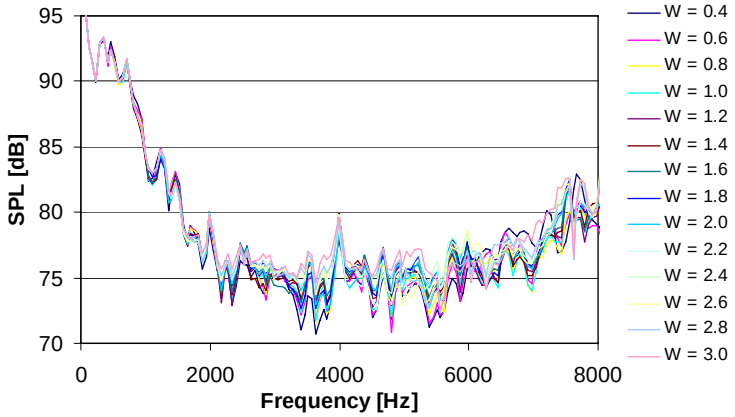

Figure 11: Integrated source powers of left engine for several values of W*; beamforming–AC*

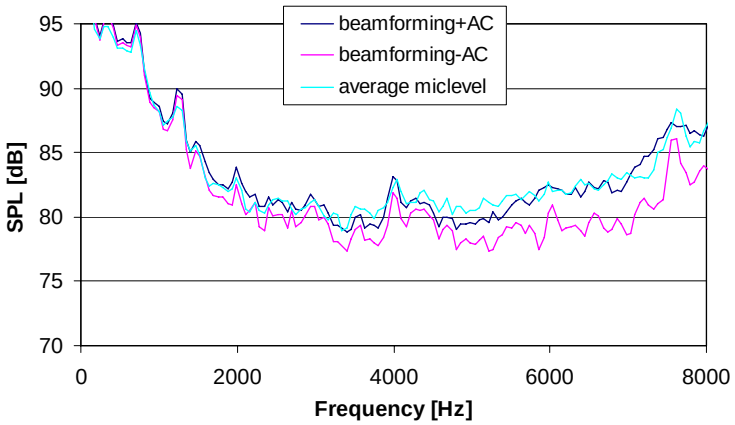

Figure 12: Integrated source powers of total area vs microphone levels; W = *1.0*

6 Application: Airbus A340

In this chapter, we apply the source power integration technique to an aircraft model with a more complicated noise source breakdown: the Airbus A340. The A340 that we consider flew over the array at an altitude of 44 m and a speed of 68 m/s. As illustrated in Figure 13, a number of integration areas was chosen, corresponding with regions of noise sources. For 17 successive time intervals of 0.1 s, corresponding to emission angles varying from 46° to 137° with respect to the flight direction, source power integration was performed on all these integration areas. Some areas in Figure 13 seem to contain no noise sources, but that of course depends on frequency and directivity angle. The source power integration technique was applied with the beamforming+AC technique (i.e., including auto-correlations), with W = 1.0 and Z = 8 dB.

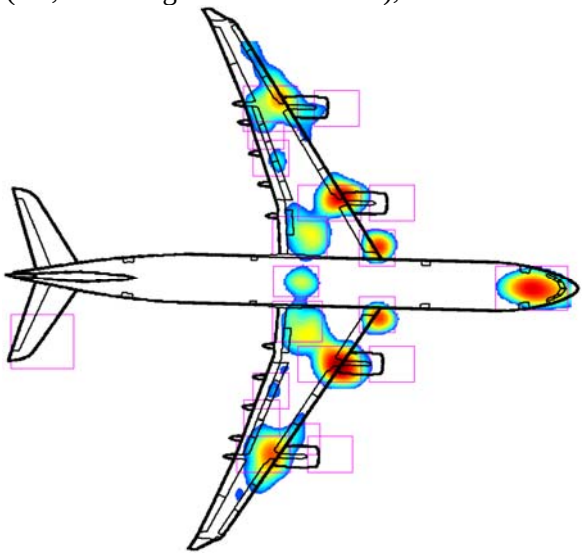

Figure 13: Acoustic image of A340 at 2000 Hz (1/3 octave band), beamforming–AC

Having calculated the integrated values for all areas, for all emission angles, and for all frequency bands, we try to acquire an overview of these results, by considering first the total SPL results, i.e., the values summed over all frequency bands. This yields a matrix of numbers, dependent on integration area and on emission angle. For each area, we then calculate (1) the maximum level, and (2) the average level over all emissions angles. Thus, we obtain numbers that depend on integration area only. From these numbers, a ranking can be made of all possible noise sources. This ranking is shown in Table 1, where the results have been scaled to Sound Power Levels (PWL), and where A-weighting was applied. This table shows that the loudest noise source is the exhaust of engine 3 (numbering from left to right).

To examine in more detail the engine 3 exhaust noise source, we can make a breakdown in 1/3 octave bands and plot the integrated results as a function of emission angle. This is done in Figure 14, in which the frequency bands are A-weighted too. This chart shows that most noise is contained in the 5000 Hz and the 6300 Hz band, with a peak at an emission angle of approximately 100°, which is slightly rearward.

The A340 example of this section demonstrates the usefulness of the source power integration technique. By making a noise source ranking, it is possible to predict how much effect noise source modifications have on the total noise emission. However, it is noted that results may be polluted as a result of the overlap that source regions may have, particularly at low frequencies. Furthermore, side lobes of a dominant source may influence the integrated results of other sources.

Table 1: Noise source ranking of A340 in landing, beamforming+AC

	Peak PWL dB(A)		Average PWL dB(A)
engine 3 exhaust	135.10	engine 3 exhaust	131.12
engine 2 exhaust	134.33	engine 2 exhaust	130.49
engine 1 exhaust	133.86	engine 1 exhaust	130.40
engine 4 exhaust	133.85	engine 4 exhaust	129.91
nose gear	131.39	nose gear	128.51
right gear	130.72	left gear	127.87
left gear	130.53	right gear	127.86
tail 2	129.80	tail 2	126.03
flap edge 4	127.80	engine 2 inlet	125.73
middle gear	127.68	engine 3 inlet	125.55
left slat horn	127.60	flap edge 4	125.34
engine 3 inlet	127.40	middle gear	125.14
flap edge 2	127.34	engine 1 inlet	125.10
right slat horn	127.30	engine 4 inlet	124.98
flap edge 3	127.23	right slat horn	124.74
engine 2 inlet	127.10	left slat horn	124.71
flap edge 1	127.06	flap edge 1	124.22
engine 4 inlet	126.97	flap edge 3	124.02
engine 1 inlet	126.42	flap edge 2	123.91
engine 4 vane	125.86	engine 4 vane	123.71

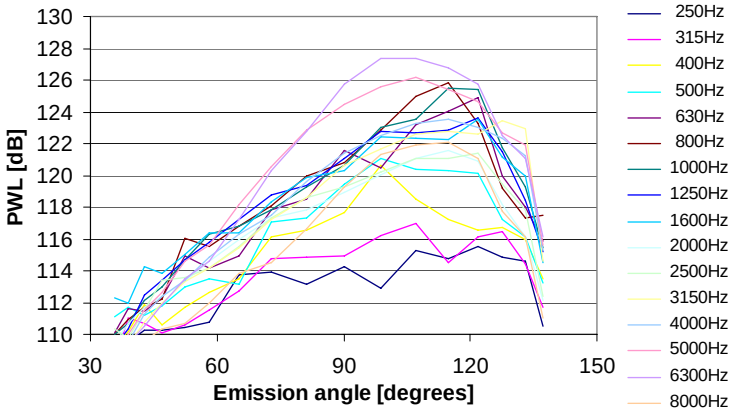

Figure 14: Source power integration results of engine 3 exhaust in PWL-dB(A); breakdown per 1/3 octave band, beamforming+AC

7 Conclusion

Application of the source power integration technique to fly-over array measurements is feasible: absolute sound emission levels can be determined from separate source regions. Herewith, a breakdown can be made of all possible noise sources on an aircraft, so that the contribution of each noise source to the total noise perceived on the ground is known. To obtain correct results, a beamforming technique that includes microphone auto-correlations must be used. Furthermore, frequency-dependent reduction of effective array aperture, as a result of coherence loss due to atmospheric turbulence, must be addressed carefully.

Acknowledgments

The fly-over array measurements at Amsterdam Airport Schiphol were performed under contract with Boeing Research & Technology Center, S.L. (Madrid, Spain).

References

1. Holthusen, H. H., and Smit, H., “A new data acquisition system for microphone array measurements in wind tunnels”, AIAA Paper 2001-2169, May 2001.
2. Sijtsma, P., Oerlemans, S., and Holthusen, H. H., “Location of rotating sources by phased array measurements”, AIAA Paper 2001-2167, NLR-TP-2001-135, May 2001.
3. Takano, Y., Horihata, K., Kaneko, R., Matsui, Y., and Fujita, H., “Analysis of sound source characteristics of Shinkansen cars by means of X-shaped microphone array”, Internoise 96, Liverpool, July 1996.
4. Barsikow, B., “Experiences with various configurations of microphone arrays used to locate sound sources on railway trains operated by the DB AG”, Journal of Sound and Vibration, Vol. 193, No. 1, May 1996, pp. 283-293.
5. Michel, U., Barsikow, B., Helbig, J., Hellmig, M., and Schüttpelz, M., “Flyover noise measurements on landing aircraft with a microphone array”, AIAA Paper 98-2336, May 1998.
6. Piet, J.-F., Michel, U., and Böhning, P., “Localization of the acoustic sources of the A340 with a large phased microphone array during flight tests”, AIAA Paper 2002-2506, May 2002.
7. Stoker, R. W., Guo, Y., Streett, C., and Burnside, N., “Airframe noise source locations of a 777 aircraft in flight and comparisons with past model-scale tests”, AIAA Paper 2003-3232, May 2003.

8. Dougherty, R. P., “Turbulent decorrelation of aeroacoustic phased arrays: Lessons from atmospheric science and astronomy”, AIAA Paper 2003-3200, May 2003.
9. Brooks, T. F., and Humphreys Jr., W. M., “Effect of directional array size on the measurement of airframe noise components”, AIAA Paper 99-1958, May 1999.
10. Sijtsma, P., and Wal, H. M. M. van der, “Identification of noise sources on civil aircraft in approach using a phased array of microphones”, NATO Paper SET-079-24, published in RTO-MP-SET-079, April 2004.
11. Dowling, A. P., and Ffowcs Williams, J. E., Sound and Sources of Sound, Wiley, 1983.
12. Tatarski, V.I., Wave Propagation in a Turbulent Medium, McGraw-Hill, 1961.